Applied Catalysis B: Environmental 126 (2012) 249–257

Contents lists available at SciVerse ScienceDirect

Applied Catalysis B: Environmental

journal homepage: www.elsevier.com/locate/apcatb

Hydrogen from scrap tyre oil via steam reforming and chemical looping in a packed bed reactor

Nikolaos Giannakeas[a], Amanda Lea-Langton[a], Valerie Dupont[a,*], Martyn V. Twigg[b]

[a] Energy and Resources Research Institute, The University of Leeds, LS2 9JT, UK
[b] Johnson Matthey Plc, Orchard Laboratory, Orchard Road, Royston SG8 5HE, UK

ARTICLE INFO

Article history:
Received 28 February 2012
Received in revised form 4 July 2012
Accepted 16 July 2012
Available online 23 July 2012

Keywords:
Scrap (waste) tyre oil
Steam reforming
Hydrogen
Chemical looping
Nickel

ABSTRACT

The production of hydrogen from scrap tyre pyrolysis oil (STPO) was investigated using catalytic steam reforming. STPO is difficult to upgrade to cleaner fuels due to its high sulphur content, complex organic composition, acidity and viscosity, which contribute to catalyst deactivation. The effects of temperature and steam to carbon ratio were investigated through thermodynamic equilibrium calculations of the main aromatic, aliphatic and hetero-N and -S compounds known to be present in STPO. The optimum operating conditions in a packed bed reactor with a Ni/Al_2O_3 catalyst at atmospheric pressure and molar steam to carbon ratio of 4:1 were 750 °C at a WHSV of 0.82 h^{-1}. The maximum hydrogen yield was 26.4 wt% of the STPO feedstock, corresponding to 67% of the maximum theoretical yield, compared to 79.4% predicted at equilibrium for a model mixture of 22 STPO compounds in the same conditions. The selectivity to the H-containing products was 98% H_2 and 2% CH_4, respectively, indicating little undesirable by-product formation, and comparable to equilibrium values. The potential to optimize the process to enhance further the H_2 yield was explored via feasibility tests of chemical looping reforming (CLR) aimed at lowering the heating and purification costs of the hydrogen production from STPO. However, the hydrogen yield decreased with each cycle of CLR. Analysis of the catalyst indicated this was most likely due to deactivation by carbon accumulation and sulphur originally present in the oil, and possibly also by trace elements (Ca, Na). The NiO particles in the catalyst were also shown to have grown after CLR of STPO. Hence further development would require pre-treating the oil for removal of sulphur, and use of a catalyst more tolerant to carbon formation.

1. Introduction

The production of hydrogen from sustainable resources and waste materials as alternatives to fossil fuels present many challenges. This is especially so when the materials consist of complex hydrocarbons and inorganic compounds, such as those in scrap tyre pyrolysis oil. Enormous quantities of scrap tyres are available, some 5×10^6 metric tonnes of scrap tyres are estimated to be produced worldwide annually, which constitute around 2% of the total solid waste produced from scrap tyres [1]. The European Union's production of scrap tyres is about 2.5×10^6 metric tonnes per year [1], and a similar amount is produced in the United States [2]. Most commonly, they are disposed of in landfill or abandoned in open areas [2], and this has high environmental impact, particularly due to fire hazards.

In comparison with wastes such as paper, glass and plastics, tyres are not an "easy" waste to treat because of their size and shape characteristics [3]. There are various options for re-using the materials present in scrap tyre including retreading, shredding and grinding, energy recovery, pyrolysis and gasification [4]. Recycling scrap tyres via a thermochemical process is suitable due to the low ash content and the higher heating value of tyres compared to coal or biomass. The high production volume of scrap tyres creates the need to find alternative waste management methods. Grinding and shredding produce rubber for applications such as carpets, sports facilities, or playgrounds [5]. Highway construction is a significant area of using scrap tyres and especially in asphalt modified with rubber produced from waste tires [6]. Eldin and Senouci [7] investigated the modification of concrete by replacing the aggregates with scrap tyre particles in terms of strength and toughness. The production of high value materials such as activated carbon was investigated by Betancur et al. [8].

The real challenge however is the production of energy from scrap tyres. Pyrolysis of scrap tyres was the first approach and the derived products are said to be relatively easily handled and transported for use in remote plants [9]. The pyrolysis products can also

* Corresponding author at: Energy Resources Institute, Energy Building, The University of Leeds, Woodhouse Lane, Leeds LS2 9JT, United Kingdom. Tel.: +44 0113 343 2503; fax: +44 0113 246 7310.
E-mail address: V.Dupont@leeds.ac.uk (V. Dupont).

0926-3373/$ – see front matter © 2012 Elsevier B.V. All rights reserved.
http://dx.doi.org/10.1016/j.apcatb.2012.07.010

Nomenclature

H_2 yield	amount of H_2 produced/amount of oil used. Units are either mol/mol or wt% of oil.
H_2 yield	ratio of H_2 yield to the maximum theoretical H_2 yield from complete steam
Eff.	reforming and water gas shift reactions (not accounting for equilibrium effects)
JM	Johnson Matthey
S:C	molar steam to carbon ratio
H-Sel	selectivity to H containing product (%)
C-Sel	selectivity to C containing product (%)
SR	steam reforming reaction (assumes CO and H_2 products)
STPO	scrap tyre pyrolysis oil
WGS	water gas shift reaction
X_{fuel}	fuel conversion fraction (based on the measurement of the CO, CO_2, CH_4 products, a nitrogen and carbon balance.
X_{H_2O}	steam conversion fraction (based on N, C and H balances)
X(model)	modelled conversion fraction of the TGA experiment, calculated using the derived kinetics using the best fit model (contracting volume) and the improved iterative Coats–Redfern method described in [10]
X(TGA)	conversion fraction during TGA experiment under N_2 flow. Defined by (mass − initial mass)/(final mass − initial mass)

be used in situ as fuels. The char produced can be used as a smokeless fuel or in activated carbon production industry [10–14]. There are currently approximately 3000 manufacturers of tyre pyrolysis plants geared towards the production of carbon black. The gaseous pyrolysis products mainly consist of CO, CO_2, H_2S, CH_4, C_2H_4, C_3H_8, C_3H_6, C_4H_{10}, C_4H_8, C_4H_6 and exhibit a very high calorific value (up to 40 MJ kg^{-1}) [6,14,15]. There is an increasing number of scrap tyre granulation plants in the world, but the larger size fraction of the granulation process (2–12 mm) does not currently have a commercial outlet, despite being produced at 60,000 tonnes/year in the EU [16]. Pyrolysis, also termed 'distillation; of the scrap tyre can offer an alternative recycling route to this fraction, with oil as a primary product and char as a by-product. The char produced from distillation of scrap tyres can also be gasified with steam and oxygen to produce a high calorific value syngas [16]. The composition of the oil produced by pyrolysis of scrap tyres reveals mainly polycyclic aromatic hydrocarbons (PAH), some carcinogenic, but also aliphatics, and hetero-N and -S hydrocarbons [5,17–19]. It has been found that by increasing the pyrolysis temperature the concentration of PAH in the oil is increased [5]. The reason for the formation of PAH was explained by Diels–Alder reactions where the cyclisation of alkenes and dehydrogenation lead to formation of the aromatic hydrocarbons [20,21]. The combustion of this type of oil produces soot that includes the unburned PAH and has an adverse impact on the environment.

Several studies investigated the use of challenging liquid feedstock derived from biomass (vegetable oil, glycerol, pyrolysis bio-oils) [22–26] and from transport waste [27] to produce hydrogen.

There are very few studies exploring the feasibility of producing H_2 from scrap tyres. Mastral et al. produced hydrogen in three stages using pyrolysis followed by oxy-gasification, and a final water gas shift step. This resulted in a H_2 yield of 6.9 wt% (solid tyre basis) from the combined pyrolysis and gasification, and 8.9 wt% after water gas shift [28]. Elbaba et al. used a novel coupled pyrolysis/catalytic steam gasification process, resulting in a H_2 yield of 5.43 wt% (solid tyre pellets basis) [29].

Portofino et al. combined a process of scrap tyre gasification followed by catalytic reforming to produce syngas. They achieved a hydrogen content of 74% in the gas when using a commercial nickel based catalyst for steam reforming at 650 °C. They also investigated a nickel–olivine catalyst for the reforming step, but found it to be less effective [30].

This study investigates an alternative use of the scrap tyre pyrolysis derived oil (STPO) as feedstock for catalytic steam reforming to produce hydrogen, and also explores the feasibility of chemical looping reforming (CLR) of STPO in a catalytic packed bed reactor.

Chemical looping steam reforming (CLR) in a packed bed reactor is a cyclic two-step process consisting of alternating feeds to a reactor containing an oxygen transfer material (OTM) and a steam reforming catalyst. In the case of a Ni-based OTM, the same material can perform well the two functions of oxygen transfer via redox cycles, and of steam reforming catalyst in its reduced form. The feeds are a fuel–steam mixture for the steam reforming/OTM reduction step, alternating with air for the oxidation step. Like the autothermal reforming process, this may result in little or no external heating. However with CLR, the syngas produced is undiluted by nitrogen, therefore the cost of an air separation unit is avoided, which represent significant capital savings. CLR can even incorporate CO_2 separation using a solid CO_2 sorbent, in which case carbonation and sorbent regeneration occur during the reforming and oxidation steps, respectively. This results in a nearly-pure H_2 product (sorption enhanced CLR) without requiring downstream water gas shift reactors, thus reducing the requirements of the final purification stage. One advantage of this process compared to the conventional steam reforming process is its scalability due to the use of a single reactor, enabling the process to be sited locally to where the hydrogen-rich syngas is required. Moreover, because the heat for the endothermic steam reforming reaction is provided internally by the oxidation and carbonation reactions, reformer designs relying on large arrays of burners are avoided, circumventing the costs of periodically replacing expensive reformer tubes. Kumar et al. [31] and Lyon and Cole [32] have shown that high purity hydrogen can be produced autothermally by using this concept in the presence of a CO_2-sorbent. It was also found that carbon formed during the fuel-steam feed step is burnt off during the OTM re-oxidation step. This feature offers the possibility of steam reforming many different types of coking feedstock heretofore not considered due to their propensity for catalyst poisoning by carbon deposition. Previous work by the authors has demonstrated high reactant conversions by chemical looping reforming using fuels such as methane [33], vegetable oil [34], waste cooking oil [22], waste automotive lubricating oil [27], and biomass pyrolysis oils (palm empty fruit bunches and pinewood) [26]. A basic requirement of the process is the ability of the fuel to reduce the OTM during the beginning of the fuel-steam feed from cycle to cycle to enable catalytic steam reforming. The ability of scrap tyre pyrolysis oil to fulfil this function has not been reported in the literature previously.

2. Experimental

2.1. Characterisation of materials

The STPO was provided by Tyrolysis Co., UK, and was produced via a fast pyrolysis process which had generated the following products distribution from the original scrap tyre: 1.1 wt% water, 8.9 wt% gas, 45 wt% oil, 31.7 wt% carbon and 13.3 wt% steel. Analysis of the CHNS content of the oil was obtained using a Flash EA1112

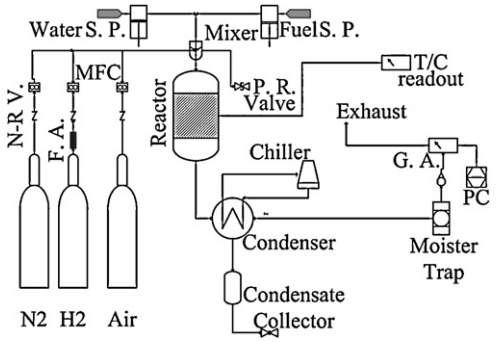

Fig. 1. Experimental set up. N-RV.: non return valve, F.A.: flame arrester, M.F.C.: mass flow controller, S.P.: syringe pump, P.R.: pressure relief, T/C: thermocouple, G.A.: gas analysers.

Elemental Analyser by CE Instruments. Inductively coupled plasma mass spectrometry (ICP-MS) analysis was carried out to determine the metal content of STPO. This was carried out with a PerkinElmer SCIEX Elan 900 after sample digestion using an Anton Paar Multiwave 3000 microwave digester. Digestion of a sample (150 mg) required about 7 ml HNO_3, 1 ml HCl and 2 ml H_2O_2. After 10 min, the mixture was loaded in the microwave digester to undergo a 4-step power programme (2 min at 1400 W–15 min at 900 W, 15 min at 1400 W ending with 15 min at 0 W fan setting 3). After digestion, the sample and a blank with no oil were left to cool in a fume cupboard, and then diluted with ultrapure water (100 ml) before transferral to the ICP-MS instrument. Thermogravimetric analysis (Shimadzu TGA 50 with TA 60 data collection software) was used to obtain the simulated distillation of the oil.

The oxygen transfer material (OTM) doubling as the steam reforming catalyst consisted of pellets of 18 wt% NiO on α-Al_2O_3 support provided by Johnson Matthey Plc (20 g). The catalyst was broken and sieved to particle size range of 0.85–2 mm prior to use.

Powder X-ray diffraction (XRD) analysis was performed to quantify the different phases present in the fresh and the used catalysts, as well as to estimate their crystal sizes. An X'Pert Philips system equipped with Highscore Plus software was used for the powder XRD data analysis. A first set of scans was carried out on the samples using a range of angles from $2\theta = 5^\circ$ to 90°, with increments of 0.017°, and scan step time of 40.7 s. A second set was performed from $2\theta = 20^\circ$ to 130°, with increments of 0.017°, and scan step time of 203.5 s. A XL30SEM Philips combined SEM with a INCA X-sight EDX (OXFORD Instruments) was used to study the morphology of the surface of the used catalyst and its elemental analysis. The specific surface area of the fresh catalyst, the catalyst after H_2 reduction and after oxidation was measured by a NOVA 2200e Quantachrome Instruments. XPS analysis was performed with a VG Escalab 250 XPS instrument. CASA XPS software was used for the analysis of the results.

2.2. Reactor set-up and test procedures

Steam reforming and chemical looping reforming experiments were performed in a quartz bench–scale reactor (Fig. 1). The feed rates of STPO and water were controlled using syringe pumps (New Era Pump Systems). The gas flows were controlled using MKS mass flow controllers, and the composition of the outlet gases were measured every 5 s using Advance Optima Analysers by ABB. Concentrations of CH_4, CO, CO_2 were measured by a Uras 14 infrared absorption analyser, H_2 by a Caldos 15 thermal conductivity analyser, and O_2 gas by a Magnos 106 paramagnetic analyser.

To prevent contamination of the products from one feed to the next, a nitrogen feed was used as a purge step in between each STPO-steam and air feed. In an industrial process, the presence of nitrogen throughout the fuel-steam feed and as a purge step would not be necessary, but would most likely be replaced by steam to prevent the possible presence of explosive mixtures. In this feasibility study, the continuous presence of N_2 allowed material balances to be performed, resulting in calculations of fuel and steam conversions, hydrogen yields, carbon and oxygen transfer rates.

2.2.1. The pre-reduction step

The fresh catalyst (supported NiO) was activated by reduction of NiO to Ni. This was achieved in the reactor by using a 5%H_2/N_2 mixture (10/200 $cm^3\,min^{-1}$ STP) at 750 °C. During this step, reaction (R1) occurred, which was evidenced by a H_2 concentration lower than 5% in the off gas. Completion of this step was confirmed when the measured off gas composition returned to 5% H_2.

$$H_2 + NiO \rightarrow H_2O + Ni \quad \Delta H_{R1,298\,K} = -2.12\,kJ\,mol^{-1} \tag{R1}$$

2.2.2. The steam reforming step: STPO-steam-N_2 feed

Steam reforming was investigated at atmospheric pressure using a molar steam to carbon ratio (S:C) of 4, at 750 °C, using 20 g of the as-received catalyst (supported NiO). The same carrier gas flow of N_2 was used as in the reduction step (200 $cm^3\,min^{-1}$ STP). Liquid feeds of STPO (0.4 ml h^{-1}, density 988 kg m^{-3}) and water (2 ml h^{-1}) at 20 °C and 1 atm were used. These conditions resulted in a weight hourly space velocity (WHSV) of 0.82 h^{-1}. Fuel and water were fed simultaneously into the top of the reactor packed with the pre-reduced catalyst directly into the hot zone to minimise the undesirable pyrolysis reactions and coking. The reactions of steam reforming ('SR' or 'R2') and water gas shift ('WGS' or 'R3') proceeded.

$$C_nH_mO_k + (n-k)H_2O_{vap} \rightarrow nCO + (n+m/2-k)H_2 \quad \Delta H_2 > 0 \tag{R2}$$

$$CO + H_2O \leftrightarrow CO_2 + H_2 \quad \Delta H_{R3,298\,K} = -41.17\,kJ\ mol^{-1} \tag{R3}$$

After approximately 1 h of steam reforming, the reactor was purged with nitrogen (200 $cm^3\,min^{-1}$ STP) until all carbon product concentrations in the off gas were zero. The experiment ended with an air feed (1000 $cm^3\,m^{-1}$STP) at 750 °C that allowed estimation of the carbon balance by burning off carbon deposits. Under the air feed the oxidation of Ni and coke oxidation are represented by reactions (R4), (R5) and (R6):

$$Ni_{(S)} + 0.5O_2 \rightarrow NiO_{(S)} \quad \Delta H_{R4,298\,K} = -239.7\,kJ\,mol^{-1} \tag{R4}$$

$$C_{(S)} + 0.5O_2 \rightarrow CO \quad \Delta H_{R5,298\,K} = -110.52\,kJ\,mol^{-1} \tag{R5}$$

$$C_{(S)} + O_2 \rightarrow CO_2 \quad \Delta H_{R6,298\,K} = -393.51\,kJ\,mol^{-1} \tag{R6}$$

2.2.3. The chemical looping steam reforming of STPO

The experiment of CLR of STPO began by a pre-reduction step under a H_2/N_2 flow as described in Section 2.2.1, followed by a series of steam reforming steps as described in Section 2.2.2. Therefore after the first cycle, reduction of the catalyst was performed by the STPO rather than H_2, according to the reaction (R7) below (also termed 'unmixed combustion'[23–25]).

$$C_nH_mO_k + (2n+m/2-k)NiO \rightarrow nCO_2 + (m/2)H_2O_{vap} + (2n+m/2-k)Ni \quad \Delta H_{R7} > 0 \tag{R7}$$

Reaction (R7) was evidenced by simultaneous production of CO_2 and H_2O with a molar ratio $2n/m$. The authors have not found evidence of unmixed partial oxidation reaction in their previous investigations of CLR with a variety of fuels on the same Ni catalyst [22,23,26,27].

Carbon deposition on the OTM-catalyst may occur during the NiO reduction (R7) until hydrogen is produced by steam reforming. This is represented by the simplified reaction (R8). The residue

might then be steam reformed or await removal during the oxidation step, or possibly react with NiO as in reactions (R9) and (R10).

$$C_nH_mO_k \rightarrow\rightarrow C_{(S)} + \sum_{d,e,f} C_dH_eO_f(+H_2, CO, H_2O, CO_2) \quad (R8)$$

$$C_{(S)} + NiO_{(S)} \rightarrow CO + Ni_{(S)} \quad \Delta H_{R9,298\,K} = 129.17\,kJ\,mol^{-1} \quad (R9)$$

$$C_{(S)} + 2NiO_{(S)} \rightarrow CO_2 + 2Ni_{(S)} \quad \Delta H_{R10,298\,K} = 85.89\,kJ\,mol^{-1} \quad (R10)$$

The STPO-steam-N_2 feed was followed by a N_2 purge (200 $cm^3\,min^{-1}$ STP and then switched to air (1000 $cm^3\,min^{-1}$ STP) to perform the oxidation step of CLR. This step featured the oxidation reactions (R4), (R5) and (R6). The air feed was turned off when the concentration of O_2 in the off-gas returned to 21 vol%, and a further N_2 purge completed a cycle. Four cycles were performed.

2.3. Process outputs via material balances

The equations for the calculation of fuel and water conversions under fuel feed, rate of NiO conversion to Ni under fuel feed, of Ni to NiO under air feed, and the rate of carbon burn-off, are described in detail elsewhere for a fuel of generic $C_nH_mO_k$ composition [22]. Fuel conversion was based on measurement of CO, CO_2 and CH_4, and water conversion was calculated from knowledge of the water input, fuel conversion and measurement of H_2 and CH_4 via a hydrogen balance. The oxygen balance provided the rate of Ni oxidation and reduction. Integration over time of the relevant rates of production/removal, yielded an estimate of the extent of Ni ↔ NiO conversion and of C deposition/burn off by the end of each cycle. The combined steam reforming and water gas shift reactions ((R2) and (R3)) provide a theoretical maximum H_2 yield of $(2n + 0.5\,m - k)$ mol of H_2 per mol of $C_nH_mO_k$ fuel, this maximum allows the calculation of a H_2 yield efficiency (experimental/theoretical maximum) and maximum water conversion ($2n - k$ per mol of fuel).

2.4. Thermodynamic equilibrium calculations on known STPO compounds

Thermodynamic equilibrium calculations were performed using minimisation of Gibbs free energy for known compounds of STPO identified from the literature [5,17–19,35]. A description of this method is given in [36]. The gas phase equilibrium of 12 aromatic, 6 aliphatic, 2 hetero-N, and 2 hetero-S compounds with water were calculated at atmospheric pressure and molar steam to carbon ratio of 4 for temperatures from 25 to 1007 °C. These were benzene, ethylbenzene, biphenyl, naphthalene, methylnaphthalene, toluene, anthracene, acenaphthene, fluorene, fulvene, D-limonene, xylenes (para/ortho/meta), cyclohexene, octane, cyclobutene, cyclobutane, pentadecane, heptadecane, heptadecane 1-nitrile, p-phenylenediamine, thiophene and benzothiophene. The thermodynamic properties were found in [37] in the required NASA polynomial format and in [38], followed by reformatting in NASA polynomial format. In addition, the H_2 yield of one of the PAHs (biphenyl) was also calculated for steam to carbon ratios between 0 and 8 to illustrate the effect of S:C on the STPO compounds in general.

3. Results and discussion

3.1. Characterisation of the oil

The properties of the STPO are summarised in Table 1 together with the techniques used to determine them.

Table 1
Characteristics of the STPO.

Property	Value	Analysis
Density	988 kg m^{-3}	
pH	6.0	
Volatiles content	96 wt%	TGA
Carbon residue	4 wt%	TGA
Ash	1.3 wt%	TGA
C	82.7 wt%	EA
H	12.1 wt%	EA
S	0.73 wt%	EA
S	0.82 wt%	ICP-MS
N	0.36 wt%	EA
O	4.11 wt%	100-EA
Metals*	1535 ppm mass	ICP-MS

List of metals and ppm mass below

B	Na	Mg	Al	Si	P
2.0	59.0	5.8	70.2	923.4	61.4
K	Ca	Ti	Fe	Zn	Br
29.5	215.5	17.1	34.7	10.7	105.7
Molar	$C_{0.35917}$	$H_{0.62499}$	$O_{0.01330}$	$N_{0.00136}$	$S_{0.00119}$
Molar mass		5.2147	g mol^{-1}		
HHV	42.8	MJ kg^{-1}			
H_f^0	−7.77	kJ mol^{-1}	−1.49	MJ kg^{-1}	STPO
$\Delta H_{R2,298\,K}$	+51.7	kJ mol^{-1}	+9.91	MJ kg^{-1}	SR of STPO
$\Delta H_{R7,298\,K}$	+34.8	kJ mol^{-1}	+6.67	MJ kg^{-1}	NiO reduction
Max H_2	Yield	39.42	wt% of STPO		
Max H_2	Yield	17.74	wt% of tyre		

The ultimate analysis allowed to derive a molar formula for the STPO ($C_{0.35917}H_{0.62499}O_{0.01330}N_{0.00136}S_{0.00119}$). There were high levels of the catalyst poison sulphur as revealed in comparable concentrations by both EA and ICP-MS (0.7–0.8 wt%), as well as significant amounts of Si and Ca. The molar formula was subsequently used to calculate the HHV of the STPO (42.8 MJ kg^{-1}) using the correlation devised by Channiwala and Parikh [39]. This in turn allowed estimating its standard enthalpy of formation ($H_f^0 = -1.49$ MJ kg^{-1}) and the standard reaction enthalpies ($\Delta H_{298\,K,R2/R7}$) of steam reforming of STPO (R2) and of reduction of NiO with STPO (R7) at +9.91 and +6.67 MJ kg^{-1}, respectively. The maximum theoretical yield of hydrogen (R2 + R3) was calculated at 39.42 wt% of the STPO feed. Using the oil yield of 45 wt% from the original scrap tyre through the fast pyrolysis process, this was equivalent to 17.74 wt% of the original scrap tyre. For a given molar steam to carbon ratio (S:C), the maximum water conversion could then be calculated, e.g. for S:C of 4, it was 49.1%.

Fig. 2 shows the STPO conversion between the extrema of mass during the volatilisation phase in the TGA of the STPO

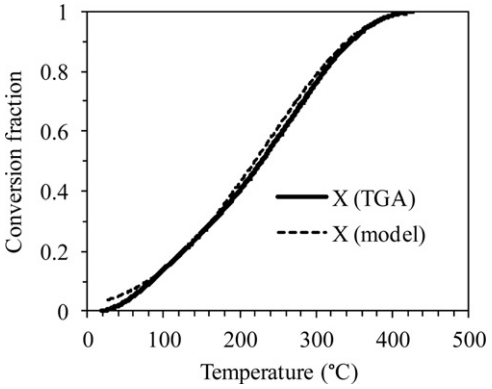

Fig. 2. Conversion fraction of STPO vs. temperature during TGA (50 ml min^{-1} N_2, 3 K min^{-1}). Kinetic model curve corresponds to contracting volume (best fit), with $A = 5.93 \times 10^{-3}$ and $E = 12.31 \pm 0.03$ kJ mol^{-1}, which produced a linear correlation of 0.9983.

(50 ml min^{-1} N_2, heating rate of 3 K min^{-1}). Modelling the volatiles' mass loss using an improved (iterative) Coats and Redfern method [40] was executed using models applicable to liquids [41]. The models tested were Avrami-Erofeev (variable order), *n*th order reaction (variable *n*), contracting volume (also called shrinking core or contracting sphere), and contracting surface. The contracting volume model generated the best fit, based on finding a linear correlation coefficient significantly closer to 1 than those of the other models (0.9983 compared to ~0.98), yielding the activation energy of 12.3 kJ mol^{-1}. The low value of this activation energy in combination with the contracting volume model indicated a physical transformation, in this case, evaporation, had taken place [41,42], as opposed to chemical reactions of thermal decomposition such as those observed for bio-oils [22,26,27]. Therefore the TGA experiment would have acted as the reverse of the condensation process that allowed collecting the oil during the fast pyrolysis of the scrap tyres in the first place, without altering the chemical mix. Fig. 2 shows the excellent agreement exhibited by the conversion vs. temperature curves obtained experimentally and by modelling.

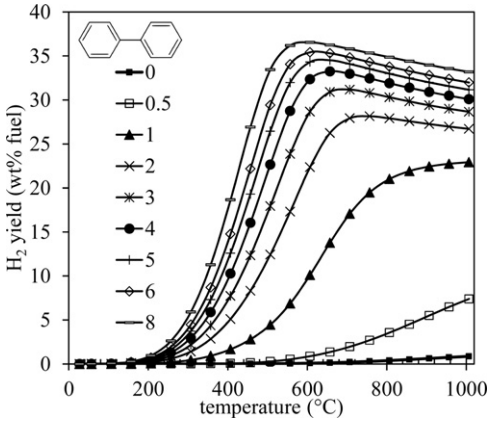

Fig. 3. H_2 yield (wt% of fuel) from biphenyl vs. temperature for S:C from 0 to 8 at thermodynamic equilibrium.

3.2. Thermodynamic equilibrium

Fig. 3 shows the effects of steam to carbon ratio on the curves of H_2 yield vs. temperature for one of the STPO model compound (biphenyl). All the main compounds tested (aromatics, aliphatics) exhibited a similar behaviour. According to Le Chatelier's principle, increasing the S:C ratio resulted in higher H_2 yields, which shifted towards lower temperatures. A compromise needed to be struck when choosing a S:C for the experiments, given the increasing costs of raising and recycling excess steam in the process. For this reason, the S:C of 4 was chosen, as increasing the S:C beyond this value did not significantly improve the yield. For each compound at S:C of 4, Table 2 lists the water conversion fraction, H_2 yield (as a wt% of the compound, and as wt% of tyre using 45% oil yield), H_2 yield efficiency (equilibrium/max theoretical), and selectivity to the H-containing products H_2 and CH_4 at equilibrium. Results are given for two temperatures: 757 °C, and the temperature where the maximum equilibrium H_2 yield was obtained. The latter varied slightly between 607 °C and 657 °C depending on the compounds (these are rough approximations since the calculations were performed with 50 °C increments). H_2 yields were in the region of 32 wt% and 36 wt% of the compound for most of the aromatics and aliphatics which are understood to form the bulk of STPO, respectively. A drop of just 1 wt% was incurred when temperature increased from 657 (maximum yield) to 757 °C (temperature of the experiments) for these compounds. The H_2 yield efficiency was of maximum 86%, and lowered to 83% at 757 °C for the same bulk of aromatic and aliphatic compounds. There were a few exceptions, such as xylenes, which had a maximum yield of 28.1 wt% at 607 °C, decreasing to 25.1 wt% at 757 °C, and heptadecane, with a maximum yield of 31.5 wt% at 607 °C, decreasing to 24.9 wt% at 757 °C. The advantage of operating at 757 °C was zero selectivity to methane compared to 0.5–1% at the temperature of maximum H_2 yield, thereby removing the unwanted CH_4 by-product, but causing some reverse water gas shift. In the selectivity calculation, H_2 is given the same weighting as CH_4. However, given that each mol of CH_4 can potentially steam reform to 4 mol of H_2, (3 if there is no CO shift), avoiding the CH_4 product appears more important than incurring a little reverse water gas shift. The hetero-N and -S compounds which typically

Table 2
Thermodynamic equilibrium conversions of the fuel (X_{fuel}) and steam (X_{H_2O}), H_2 yield, H_2 yield efficiency and the selectivity to the H-containing products (H_2 and CH_4) for S:C = 4 and known STPO compounds. Rows 1 and 2: calculated averaged values (±stdev) over 12 aromatics[a]. Rows 3 and 4: same over 6 aliphatic compounds[b]. Rows 5 and 6: same over 4 hetero-N and -S compounds[c]. Max H_2 yield was found at ~657 °C for all compounds except xylenes, heptadecane and the hetero-N and -S compounds (~607 °C). Last row corresponds to STPO mixture (from Table 3 in [19]), accounting for 77.8% area of GC–MS peaks out of the 91.3% listed).

Compounds and temperature	X_{H_2O}	H_2 yield wt% fuel	H_2 yield wt% tyre	H_2 yield eff. %	H-Sel H_2%	H-Sel CH_4%
Aromatics						
@757 °C	0.394 ± 0.02	32.0 ± 0.9	14.5	82.7 ± 3.1	99.9 ± 0.0	0.1 ± 0.0
@657 °C (Max H_2 yield)	0.415 ± 0.01	33.0 ± 0.7	14.9	85.7 ± 0.1	99.5 ± 0.0	0.5 ± 0.0
Xylenes @757 °C	0.301	25.1	11.3	62.8	100.0	0.0
Xylenes @607 °C (Max yield)	0.349	28.3	12.7	70.9	99.0	1.0
Aliphatics						
@757 °C	0.389 ± 0.004	36.0 ± 1.0	16.2	83.4 ± 0.1	99.9 ± 0.1	0.1 ± 0.0
@657 °C (Max H_2 yield)	0.404 ± 0.07	36.7 ± 1.3	16.5	86.0 ± 0.1	99.5 ± 0.2	0.5 ± 0.2
Heptadecane@757 °C	0.268	24.9	11.2	57.1	99.9	0.1
Heptadecane@607 °C (Max yield)	0.348	31.5	14.2	72.1	98.5	1.5
Hetero-N–S						
Heptadecane-1-nitrile @757 °C	0.276	23.43	10.5	58.1	100.0	0.00
Heptadecane-1-nitrile @607 °C	0.356	29.70	13.4	73.6	98.5	1.45
p-Phenylenediamine @757 °C	0.305	17.90	8.06	59.8	100.0	0.00
p-Phenylenediamine @607 °C	0.382	22.74	10.2	76.1	98.6	1.42
Thiophene @757 °C	0.290	12.74	5.73	53.1	88.8	0.00
Thiophene @607 °C	0.407	16.94	7.62	70.5	87.7	0.97
Benzothiophene @757 °C	0.307	16.95	7.63	59.3	96.3	0.00
Benzothiophene @607 °C	0.402	21.63	9.73	75.6	93.2	1.19
STPO mixture @757 °C	0.376	31.53	14.2	79.4	99.8	0.1

[a] Benzene, ethylbenzene, biphenyl, naphthalene, methylnaphthalene, toluene, anthracene, acenaphthene, fluorene, fulvene, D-limonene, p/o/m-xylene.
[b] Cyclohexene, octane, cyclobutene, cyclobutane, pentadecane, heptadecane.
[c] Hetero-N: heptadecane-1-nitrile, p-phenylenediamine, hetero-S: thiophene and benzothiophene.

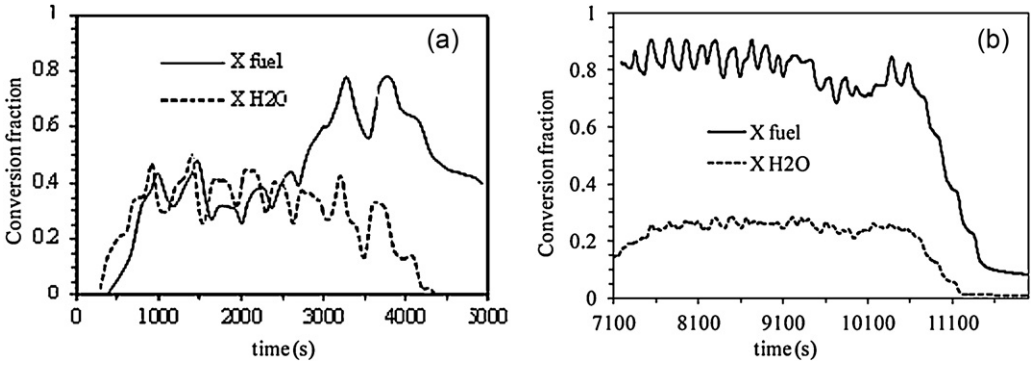

Fig. 4. Conversion fractions (X_{fuel}) and steam X_{H_2O} vs. time on stream at (a) 600 °C and (b) 750 °C for S:C of 4.

account for a few wt% in STPO [19]) had lower H_2 yields and were more sensitive to temperature, given that their maximum H_2 yield occurred at around 607 °C. Simulation of a STPO mixture at 757 °C such as that described in Table 3 of [19], generated a H_2 yield of 31.5 wt% of mixture, with a H_2 yield efficiency of 79.4%. When converting the H_2 yield to the original scrap tyre feedstock via the oil yield of 45 wt% from pyrolysis, this became 14.2 wt% of the original scrap tyres. These values as well as the water conversion fraction of 0.376 and the selectivity to H-products (99.8% H_2, 0.1% CH_4) can then form the basis of a comparison with our experimental results.

3.3. Catalytic steam reforming of STPO

Fig. 4 shows a plot of the STPO and steam conversions during the STPO-steam-N_2 phase at 600 °C (4a) and 750 °C (4b) for a S:C ratio of 4. At 600 °C, the conversion of the oil first stabilised at around 37% for 2000 s, and increased subsequently to 68% for a further 1000 s. Steam conversions were 37% and 26% in the same time ranges respectively, compared to the maximum theoretical steam conversion of 48.1% at S:C ratio of 4. This corresponded to H_2 yields of 23.6 and 20.9 wt%, respectively. Increasing the reactor temperature to 750 °C generated more stable fuel and steam conversions (Fig. 4b), despite unfavourably shifting the water gas shift equilibrium (R3). The average STPO conversion at 750 °C was 82%, while the conversion of the steam was 24%. Hydrogen yield for this experiment was around 23 wt% (or 58% H_2 yield efficiency). These experiments showed STPO can be steam reformed over a Ni catalyst with good fuel and steam conversions. Subsequently the CLR experiments were carried out at 750 °C.

3.4. Chemical looping reforming of STPO

Fig. 5 charts the amounts of H_2, CO_2, CO and CH_4 (dry basis) with time in the reformate at 750 °C for a S:C ratio of 4. Cycle 2 was chosen as representative. In any given cycle, two consecutive regimes could be identified during a STPO-steam-N_2 feed, as was found in [27,26]. At the beginning (3000–6000 s), CO_2 was the main product, and CO, CH_4 and H_2 concentrations were negligible. Following this, there was a simultaneous production of significant levels of CO_2, CH_4, CO, with H_2 as the main product.

Fig. 6 displays the STPO and steam conversions of cycle 2 calculated from carbon and hydrogen balances using the measured concentrations in Fig. 5. The first regime was attributed to NiO reduction (R7) because CO_2 was the only gas product with a negative steam conversion (−15%) and significant fuel conversion (~80%). During this regime, the ratio of production of CO_2 and H_2O was 1.20 ± 0.02 (average over 1500 s), compared to the theoretical ratio $2n/m$ of 1.15 from stoichiometry of reaction (R7). This

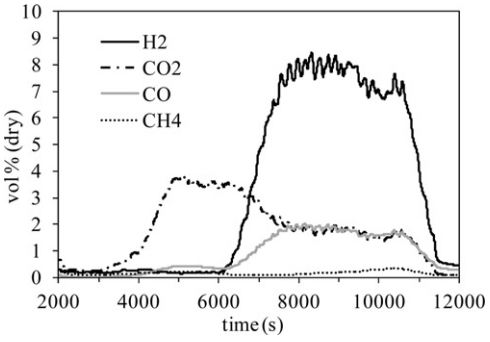

Fig. 5. H_2, CO_2, CO and CH_4 vol% in the dry reformate vs. time on stream from the chemical looping reforming of STPO at S:C = 4 and 750 °C. Balance to 100 vol.% attributed to N_2 gas carrier, cycle 2.

confirmed the almost exclusive reduction of NiO by STPO (unmixed combustion). The second regime (beyond 6000 s) was attributed to steam reforming with water gas shift ((R2) and (R3)). The products were CO, CO_2, H_2, with a positive steam conversion (+25%) and a conversion of STPO around 85%. There were also small amounts of CH_4, indicating activity of the methanation of CO (reverse R2 producing CH_4), or thermal cracking (R8), or a combination of both (R2) and (R8). This behaviour is typically found when the steam reforming catalyst activity is low, most probably caused by catalyst poisoning due to the high levels of sulphur in the feed.

The extent of NiO reduction to Ni was calculated for each STPO-H_2O-N_2 feed and subsequent N_2 purge (Fig. 7), yielding the total NiO conversion to Ni for each cycle. There was no evidence of reduction during the N_2 purge (lack of reactions (R9) and (R10)), consistent with complete reduction during the preceding STPO-H_2O-N_2 feed. Similarly, the rate of Ni oxidation to NiO was determined via carbon

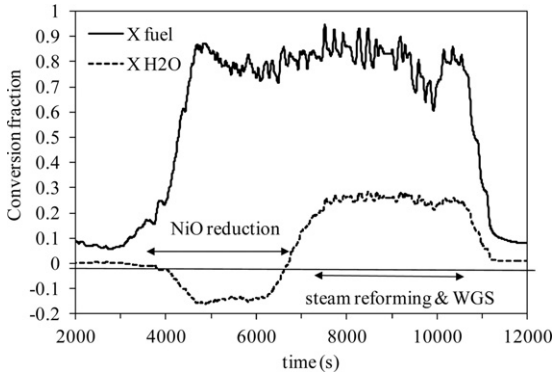

Fig. 6. Conversion of oil and water vs. time on stream during fuel-steam feed step, S:C = 4, T = 750 °C, cycle 2.

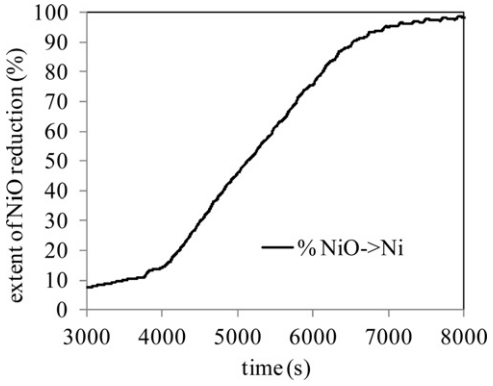

Fig. 7. NiO reduction vs. time (% of NiO fresh catalyst), S:C = 4, T = 750 °C, cycle 2.

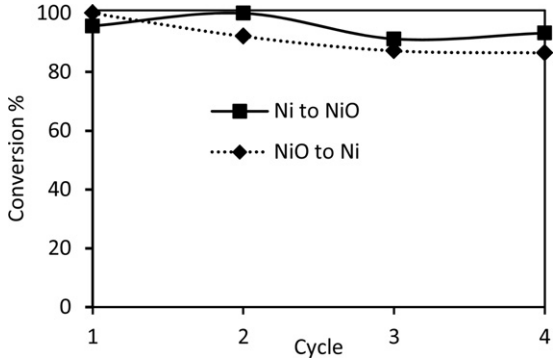

Fig. 8. Extent of NiO conversion to Ni, and of Ni oxidation to NiO for each cycle.

and oxygen balances for each air feed. After integration, the extent of Ni oxidation to NiO was calculated for each cycle (Fig. 8).

Close to 100% oxidation of Ni and 100% reduction of NiO were maintained from cycle to cycle, with closely matching amounts of O transferred between reduction and oxidation. This indicated STPO has the ability to reduce the Ni catalyst and the catalyst is able to re-oxidise repeatedly, as required for successful chemical looping.

Table 3 records the average H_2 yields and H_2 yield efficiencies, alongside the percentage fuel and steam conversions (X_{fuel} and X_{H_2O}), selectivity to H-products and the carbon balance (in g of C) for the 4 CLR cycles. The mass of carbon listed as 'balance' results from the difference between carbon assumed deposited during the catalyst reduction regime of the fuel/steam feed (difference to 100% of the fuel conversion) and the carbon burned to CO and CO_2 during the catalyst oxidation regime (air feed).

The highest H_2 yield was obtained in cycle 1 with 26.4 wt% of STPO, or 11.9 wt% of original scrap tyre, corresponding to a H_2 yield efficiency of 67%. The yield of 11.9 wt% of scrap tyre is the highest reported for scrap tyre conversion to hydrogen and was maintained for the whole duration of the first cycle (2900 s). Some of the penalty in efficiency (difference to 100%) was caused by the reverse water gas shift reaction at the relatively high temperature of 750 °C. This is corroborated by the selectivity to CO being greater than to CO_2, with a CO to CO_2 ratio of ca. 1.5 (from Fig. 5). Moreover, the incomplete

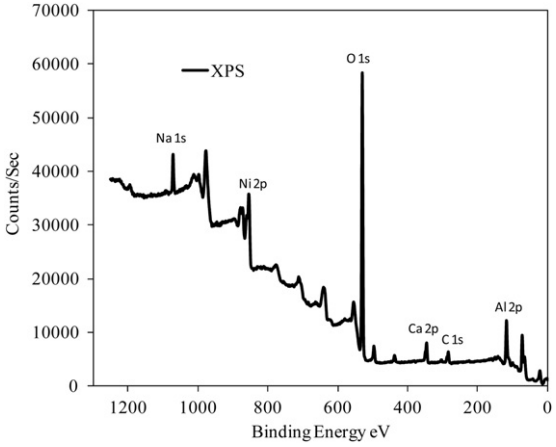

Fig. 9. XPS analysis of used NiO catalyst (cycle 4).

fuel conversion (86.4%) was responsible for the largest penalty in H_2 yield efficiency, as well as the expected equilibrium limit (79.4% according to the model STPO mixture, Table 2). Therefore the mean measured H_2 yield could be further improved by above all carrying out a better fuel conversion through reaction (R2). This may be achieved using a lower WHSV than that used in the experiment, by using lower flow rates or a larger mass of catalyst. This could not be tested in the present set-up due to practical constraints. It is however clear that STPO has a good potential as a feedstock for catalytic steam reforming.

However the H_2 yield decreased with each subsequent cycle of chemical looping reforming, reaching about 50% of the initial cycle value by the 4th cycle. This drop in H_2 yield was reflected in declining STPO and steam conversions from 86% and 29% to 70% and 12%, respectively. At the same time the selectivity to the H-containing product CH_4 was also seen to increase from 2.4% to 28.1% from cycles 1 to 4 (Table 3). These effects reflect a decrease of catalyst activity for both steam reforming and water gas shift reactions ((R2) and (R3)), allowing thermal cracking to become increasingly important.

3.5. Causes of catalyst deactivation

There are several possible causes for the catalyst deactivation. Catalyst coking is a known deactivation mode during steam reforming. The carbon balances listed in Table 3 showed the amount of carbon increased with each cycle.

By the 4th cycle, approximately 0.22 g of carbon (i.e. 1.1 wt% of the catalyst) were estimated to have deposited on the catalyst, representing 1.83×10^{-2} mol of C, for a catalyst bed that contained just 4.82×10^{-2} mol of Ni to start with.

Fig. 9 plots the XPS elemental scan of the used catalyst after the CLR experiments that concluded with an air feed and a final N_2 purge.

Although the sample had been oxidised, there was evidence of carbon on the surface of the catalyst from the XPS. The carbon peak at 284 eV corresponds to Ni_3C (nickel carbide) [43], and formation of nickel carbide on steam reforming catalysts is a known cause

Table 3
Conversions of the STPO and steam, H_2 yield, H_2 yield efficiency, selectivity to the H-containing products (H_2 and CH_4) and carbon balance at 750 °C for S:C = 4 for four CLR cycle experiments.

Cycle	X_{fuel}	X_{H_2O}	H_2 yield wt% STPO	H_2 yield wt% tyre	H_2 yield Eff %	H-Sel H_2%	H-Sel CH_4%	C-balance (g)
1	0.864	0.289	26.4	11.9	67	97.6	2.4	0.0391
2	0.816	0.239	22.3	10.0	55	93.1	6.9	0.012
3	0.603	0.197	16.4	7.4	42	88	12.1	0.0953
4	0.696	0.118	13.1	5.9	33	72	28.1	0.2189

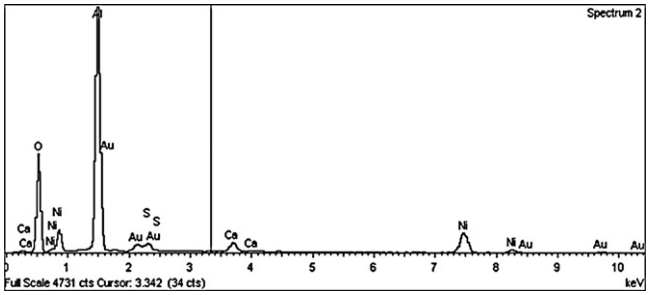

Fig. 10. EDX spectrum focused on SEM image of catalyst particle of used catalyst (cycle 4).

of deactivation for which [44–46] provide few examples of the extensive literature on the subject. The XPS spectrum also showed Ca and Na were on the used catalyst. Calcium was present in significant concentration in the STPO (215 ppm, Table 1), and to a lower level, sodium too (59 ppm). Calcium deposition is detrimental to catalyst performance [47], and sodium can also decrease catalyst activity. SEM-EDX analysis (Fig. 10) showed the expected Al, Ni and O peaks, and also the presence of Ca and sulphur, present in large concentration in the STPO (8249 ppm, Table 1). Sulphur is a powerful poison of nickel during steam reforming [48–50].

Finally, deactivation can also be caused by loss of surface area caused by sintering of the active metal crystallites. Powder XRD analysis using Rietveld refinement was used to determine metal particle size and composition (Fig. 11). Agreement between observed and modelled spectra was very good (residual curve close to zero). The phase compositions derived from Rietveld refinement via the Scherrer equation (corrected for strain and instrumental peak broadening) yielded 17.8 wt% NiO and 79.2 wt% α-Al_2O_3 for both the fresh and used catalysts, thus placing them very close to the 18 wt% NiO/82 wt% Al_2O_3 given by the manufacturer. Thus deactivation via loss of the active metal was negligible. Comparison of the NiO crystallite size of 45 nm for the fresh catalyst and 73 nm for the used oxidised catalyst indicated some sintering of the NiO particles.

The catalyst deactivation appears to have been a combination of coking, nickel carbide formation, poisoning by the sulphur (and perhaps Ca and Na contents), and some sintering of the active metal particles crystallites. The first step in controlling catalyst deactivation would be to desulphurise the STPO, perhaps by hydrodesulphurisation (HDS) [41], and secondly reduce coking by more careful addition of STPO to the steam reforming reactor.

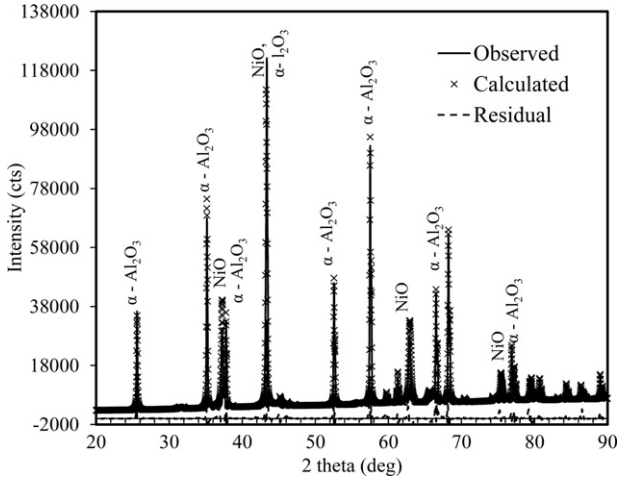

Fig. 11. Rietveld refinement of XRD spectrum of used catalyst (S:C 4, cycle 4).

4. Conclusions

Steam reforming of scrap tyre pyrolysis oil (STPO) was possible between 600 and 750 °C, with the higher temperature yielding more stable products over time. Using a nickel catalyst that had been pre-reduced in H_2/N_2, afforded good H_2 yields (26 wt% of the oil feed or 11.8 wt% of the tyre), achieved via oil and steam conversions of 86% and 26%, respectively. Whereas steam conversion was limited by the water gas shift equilibrium, conversion of the oil has the potential to be improved by increasing the residence time in the reformer or increasing the amount of catalyst used. The ability of the STPO to repeatedly reduce the NiO to catalytically active Ni, and for the catalyst to be re-oxidised by air, as required for chemical looping reforming, was also demonstrated. Catalyst deactivation during chemical looping reforming of STPO was caused by accumulation of carbon on the catalyst, nickel carbide formation, and poison accumulation (sulphur, calcium and sodium). There was also evidence of sintering of the nickel phases. Future work will focus on investigating potential refining processes of this fuel to overcome the more important deactivation factors and the incorporation of a CO_2 solid sorbent to enhance the oil and steam conversion and hence the H_2 yield while also increasing the H_2 purity in the syngas.

Acknowledgements

The RCUK for grants EP/D078199/1 and EP/G01244X/1, Johnson Matthey Plc for providing the catalyst and Jon Radford at Tyrolysis Co. for providing the scrap tyres pyrolysis oil.

References

[1] C. Berrueco, E. Esperanza, F.J. Mastral, J. Ceamanos, P. García-Bacaicoa, Journal of Analytical and Applied Pyrolysis 74 (2005) 245–253.
[2] C. Roy, A. Chaala, H. Darmstadt, Journal of Analytical and Applied Pyrolysis 51 (1999) 201–221.
[3] J.A. Conesa, A. Fullana, R. Font, Energy & Fuels 14 (2000) 409–418.
[4] G. Ramos, F.J. Alguacil, F.A. Lopez, Revista de Metalurgica (Madrid) 47 (2011) 273–284.
[5] A.M. Cunliffe, P.T. Williams, Journal of Analytical and Applied Pyrolysis 44 (1998) 131–152.
[6] J.A. Epps, National Cooperative Highway Research, Uses of Recycled Rubber Tires in Highways, National Academy Press, Washington, DC, 1994.
[7] N.N. Eldin, A.B. Senouci, Journal of Materials in Civil Engineering 5 (1993) 478–496.
[8] M. Betancur, J.D. Martínez, R. Murillo, Journal of Hazardous Materials 168 (2009) 882–887.
[9] P.T. Williams, S. Besler, D.T. Taylor, Fuel 69 (1990) 1474–1482.
[10] H.S.W. Kaminsky, in: S.B.R.J.L. Jones (Ed.), Thermal Conversion of Solid Wastes and Biomass, American Chemical Society Publishers, Washington, DC, 1980.
[11] C. Roy, B. Labrecque, B. de Caumia, Resources Conservation and Recycling 4 (1990) 203–213.
[12] B. Bilitewski, G. Hardtle, K. Marek, in: K.M.G.L. Ferrero, A. Buekens, A.V. Bridgwater (Eds.), Pyrolysis and Gasification, Elsevier Applied Science, London, 1989.
[13] G. Collin, in: S.B.R.J.L. Jones (Ed.), Thermal Conversion of Solid Wastes and Biomass, American Chemical Society Publishers, Washington, DC, 1980.
[14] B. Sahouli, S. Blacher, F. Brouers, H. Darmstadt, C. Roy, S. Kaliaguine, Fuel 75 (1996) 1244–1250.
[15] I. de Marco Rodriguez, M.F. Laresgoiti, M.A. Cabrero, A. Torres, M.J. Chomón, B. Caballero, Fuel Processing Technology 72 (2001) 9–22.
[16] F.A. Lopez, T.A. Centeno, F.J. Alguacil, B. Lobato, A. Lopez-Delgado, J. Fermoso, Waste Management 32 (2012) 743–752.
[17] B. Benallal, C. Roy, H. Pakdel, S. Chabot, M.A. Poirier, Fuel 74 (1995) 1589–1594.
[18] M.R. Islam, H. Haniu, M.R.A. Beg, Fuel 87 (2008) 3112–3122.
[19] F.A. Lopez, T.A. Centeno, F.J. Alguacil, B. Lobato, Journal of Hazardous Materials 190 (2011) 285–292.
[20] G.L. Ferrero, K. Maniatis, A. Buekens, A.V. Bridgwater, Pyrolysis and Gasification, Elsevier Applied Science, London, 1989.
[21] P.T. Williams, D.T. Taylor, Fuel 72 (1993) 1469–1474.
[22] P. Pimenidou, G. Rickett, V. Dupont, M.V. Twigg, Bioresource Technology 101 (2010) 6389–6397.
[23] P. Pimenidou, G. Rickett, V. Dupont, M.V. Twigg, Bioresource Technology 101 (2010) 9279–9286.
[24] B. Dou, G.L. Rickett, V. Dupont, P.T. Williams, H. Chen, Y. Ding, M. Ghadiri, Bioresource Technology 101 (2010) 2436–2442.

[25] B. Dou, V. Dupont, G. Rickett, N. Blakeman, P.T. Williams, H. Chen, Y. Ding, M. Ghadiri, Bioresource Technology 100 (2009) 3540–3547.
[26] A. Lea-Langton, R.M. Zin, V. Dupont, M.V. Twigg, International Journal of Hydrogen Energy 37 (2012) 2037–2043.
[27] A. Lea-Langton, N. Giannakeas, G.L. Rickett, V. Dupont, M.V. Twigg, SAE International Journal of Fuels Lubricants 3 (2010) 810–818.
[28] A.M. Mastral, R. Murillo, T. Garcıía, M.V. Navarro, M.S. Callen, J.M. López, Fuel Processing Technology 75 (2002) 185–199.
[29] I.F. Elbaba, C. Wu, P.T. Williams, Energy & Fuels 24 (2010) 3928–3935.
[30] S. Portofino, S. Casu, P. Iovane, A. Russo, M. Martino, A. Donatelli, S. Galvagno, Energy & Fuels 25 (2011) 2232–2241.
[31] R.V. Kumar, J.A. Cole, R.K. Lyon, Unmixed Reforming An Advanced Steam Reforming Process 218th. ACS National Meeting, New Orleans, 1999, pp. 894–898.
[32] R.K. Lyon, J.A. Cole, Combustion and Flame 121 (2000) 249–261.
[33] V. Dupont, A.B. Ross, E. Knight, I. Hanley, M.V. Twigg, Chemical Engineering Science 63 (2008) 2966–2979.
[34] V. Dupont, A.B. Ross, I. Hanley, M.V. Twigg, International Journal of Hydrogen Energy 32 (2007) 67–79.
[35] M.R. Islam, M.S.H.K. Tushar, H. Haniu, Journal of Analytical and Applied Pyrolysis 82 (2008) 96–109.
[36] R. Md Zin, A. Lea-Langton, V. Dupont, M.V. Twigg, International Journal of Hydrogen Energy 37 (2012) 10627–10638.
[37] C.K. Westbrook, W.J. Pitz, H.J. Curran, M. Mehl, Isocetane version of newtherm15.dat, <https://www-pls.llnl.gov>, 2009.
[38] C.L. Yaws, Yaw's Handbook of Thermodynamic and Physical Properties of Chemical Compounds, 2003.
[39] S.A. Channiwala, P.P. Parikh, Fuel 81 (2002) 1051–1063.
[40] E. Urbanovici, C. Popescu, E. Segal, Journal of Thermal Analysis and Calorimetry 58 (1999) 683–700.
[41] S. Vyazovkin, J.S. Clawson, C.A. Wight, Chemistry of Materials 13 (2001) 960–966.
[42] S. Kim, D. Kavitha, T.U. Yu, J.-S. Jung, J.-H. Song, S.-W. Lee, S.-H. Kong, Journal of Analytical and Applied Pyrolysis 81 (2008) 100–105.
[43] S. Sinharoy, L.L. Levenson, Thin Solid Films 53 (1978) 31–36.
[44] C.H. Bartholomew, Applied Catalysis A: General 212 (2001) 17–60.
[45] H.H. Hwu, B. Fruhberger, J.G. Chen, Journal of Catalysis 221 (2004) 170–177.
[46] S. Lee, G. Keskar, C. Liu, W.R. Schwartz, C.S. McEnally, J.-Y. Kim, L.D. Pfefferle, G.L. Haller, Applied Catalysis B: Environmental 111/112 (2012) 157–164.
[47] S.Y. Christou, S. García-Rodríguez, J.L.G. Fierro, A.M. Efstathiou, Applied Catalysis B: Environmental 111/112 (2012) 233–245.
[48] J.A. Rodriguez, Progress in Surface Science 81 (2006) 141–189.
[49] M.M. Yung, J.N. Kuhn, Langmuir 26 (2010) 16589–16594.
[50] Y.S. Chen, C. Xie, Y. Li, C.S. Song, T.B. Bolin, Physical Chemistry Chemical Physics 12 (2010) 5707–5711.